Thermochimica Acta, 226 (1993) 281–299
Elsevier Science Publishers B.V., Amsterdam

Evaluation of doped polyethylene oxide as solid electrolyte [1]

Anil K. Sircar [a,*], Peter T. Weissman [a], Binod Kumar [a] and R.A. Marsh [b]

[a] *Center for Basic and Applied Polymer Research, University of Dayton, Dayton, OH 45469-0130 (USA)*

[b] *Aeropropulsion and Power Directorate, Wright-Patterson Air Force Base, OH 45433-6533 (USA)*

(Received 24 November 1992; accepted 19 April 1993)

Abstract

A study correlating electrical properties (a.c. conductivity and permittivity) to changes in the polymer morphology of polyethylene oxide (PEO) doped with lithium tetrafluoroborate ($LiBF_4$) was investigated. A TA Instruments Dielectric Analyzer, DEA 2970, was used to measure electrical properties. The morphological changes were traced via differential scanning calorimetry (DSC), thermogravimetry (TG), and Fourier transform infrared spectroscopy (FTIR).

The study showed that the relationship between dopant concentration and morphological changes of the polymer is rather complex. A reduction of crystallinity at low dopant concentration, phase separation involving ion–polymer complexes at high concentration, and formation of neutral ion pairs at very high ion concentration are the proposed mechanisms to explain the conductivity data. The dissociation of ions, changes in viscosity, and their effect on ion mobility were also considered to explain conductivity and permittivity data.

The advantages and limitations of the DEA 2970 for measuring the ionic conductivity of polymeric electrolytes are discussed.

INTRODUCTION

Polymer-based electrolytes are gaining increasing importance in solid-state electrochemistry in view of their potential applications, the most important of which is high energy density batteries. Armand et al. [1] have reported the basic properties of a poly(ethylene oxide)–lithium salt electrolyte. Since then, polymer electrolytes based on complexes formed between PEO and alkali metal salts have become materials of considerable interest due to their desirable conductivity, mechanical properties, and compatibility with lithium electrodes. In addition, their processing and

* Corresponding author.

[1] Presented at the 21st Annual NATAS Conference, Atlanta, GA, 13–16 September 1992.

0040-6031/93/$06.00 © 1993 – Elsevier Science Publishers B.V. All rights reserved

fabrication in thin film configurations are relatively simple. However, their ionic conductivity (10^{-7}–10^{-8} S cm^{-1}) at ambient temperature considerably limits their application.

To understand the conductivity behavior of the PEO–alkali metal salt system, it is necessary first to undestand its phase behavior. Two or more phases, e.g. crystalline polymer, amorphous polymer, crystalline complex, amorphous complex, and crystalline salt, may coexist with one another. Moreover, the ratio of different phases depends on the PEO:dopant ratio, and the time interval and temperature of the measurement, as well as the polymer characteristics such as molecular weight, molecular weight distribution, completeness of crystallization, and the kinetics of crystallization [2]. Different techniques including DSC [3–6], X-ray diffraction [7–9], optical microscopy [10], electron microscopy [11], nuclear magnetic resonance (NMR) [12, 13], and infrared spectroscopy (IR) [14] have been used to determine the phase diagrams and structural characteristics of polymer–salt complexes with variable success.

In the present study, attempts have been made to correlate the phase changes observed by DSC and TG with the electrical behavior (conductivity, permittivity) as determined by DEA, using a PEO–$LiBF_4$ polymeric electrolyte system. As Fauteux [2] concedes, there is difficulty in comparing literature data because experimental differences exist among different studies. Supporting data for the structural changes have been obtained by IR measurements. These measurements have been carried out as a function of dopant concentration and temperature, which have considerable effect on the phase relations and, consequently, on the conductivity of the electrolyte.

EXPERIMENTAL

Materials

Polyox N750, supplied by Union Carbide, was used for PEO. The number average molecular weight reported by the manufacturer is 300,000. Manufacturer's literature reports that it contains ≈3% fumed silica. The polymer was used without further purification. The melting point T_m of the sample, as determined by differential scanning calorimetry (DSC) peak enthalpy values T_p, was 68.5°C. Lithium tetrafluoroborate ($LiBF_4$) was chosen as the dopant because of its low lattice energy.

Preparing films

Films containing the dopant were cast in a Teflon mold from solutions containing the components in the desired ratio in acetonitrile and dried under partial vacuum at room temperature for 24 h. These were used for

DSC and thermogravimetry/derivative thermogravimetry (TG/DTG) experiments. The films were very hygroscopic and were stored in a vacuum desiccator until needed. Once the vacuum desiccator was opened, it was necessary to wait another 24 h before the enclosed films in the desiccator were relatively free of moisture. For conductivity and permittivity measurements, films were cast on to the electrode itself to avoid contact resistance. Good reproducibility of conductivity data was observed for a sample which was repeated three times.

Dielectric measurements

Dielectric analysis by the TA Instruments DEA 2970 measures the capacitance and conductance of a material as a function of time, temperature and frequency. This provides valuable information about molecular motion, including the permittivity, E', and loss factor, E''. In simple terms, E' represents the degree of alignment of the dipoles to the electric field. The loss factor E'' measures the amount of energy required to align the dipoles or to move ions and can be expressed as

$$E'' = E''_{\mathrm{d}} + \frac{\partial}{\omega e_0} \tag{1}$$

where E''_{d} is the energy loss due to dipole orientation, ∂ the ionic conductivity, ω the angular frequency, and e_0 the absolute permittivity of the free space ($8.85 \times 10^{-14}\,\mathrm{F\,cm^{-1}}$). For high ionic conductivity, E''_{d} is negligible and ∂ is derived from the loss factor

$$\partial = E''\omega e_0 \tag{2}$$

The TA Instruments DEA 2970 is capable of operating between −150 and 500°C and has a reported ionic conductivity measurement range from 10^{-17} to $10^{-2}\,\mathrm{S\,cm^{-1}}$ [15] in the frequency range 0.003 Hz–100 kHz. It is capable of scanning 28 different frequencies in one experiment and can operate in a programmed heating or cooling mode. The electrode assembly is confined in a glass dome (which offers protection from humid air) and can be operated under vacuum or in the presence of a purge gas. A single-surface electrode was used to avoid the complication with the more common parallel electrode due to thickness changes during programmed heating to high temperatures (up to 200°C) as the sample melts. The electrode was calibrated before each measurement. A heating rate of $1\,^{\circ}\mathrm{C\,min^{-1}}$ under nitrogen purge was used for these experiments.

DSC measurements

The melting temperature and relative crystallinity (as measured by enthalpy) of doped and undoped PEO were determined by a TA Instruments 2910 DSC at a heating rate of $10\,^{\circ}\mathrm{C\,min^{-1}}$ under nitrogen

purge. Pure indium was used for temperature and enthalpy calibration. The sample was weighed and put back in the vacuum desiccator for a minimum of 4 h before the DSC experiment to remove moisture absorbed during weighing. The parameters measured from the DSC endotherms are enthalpy ΔH_m, temperature of origin of the endotherm T_o, peak temperature T_p, and temperature of the end of the endotherm T_e.

Thermogravimetry

A TA Instruments 2950 TGA, temperature-calibrated with indium wire, was used. Samples were run at 10°C min^{-1} under nitrogen.

IR Spectroscopy

Infrared (IR) vibrational spectra were obtained using a Nicolet SX60 FTIR spectrometer. The polymer specimen was dissolved in acetonitrile. A thin film suitable for IR transmission measurement was prepared by placing three to four drops of the solution on an AgCl crystal. The solvent was allowed to evaporate in a hood. The specimen was kept in a vacuum desiccator for 12 h, then transferred into a dry box and kept there for an additional 24 h before measurement.

RESULT AND DISCUSSION

DSC studies

Table 1 and Figs. 1 and 2 show the results of DSC experiments of the PEO/$LiBF_4$ samples with varying concentrations of salt. Table 1 sumarizes the data (T_o, T_p, T_e, and ΔH_m) of the DSC experiments. Three different stages are observed as the salt concentration increases progressively from PEO to the lithium salt. A sharp drop in T_o, T_p, T_e and ΔH_m is observed during the first stage (up to O:Li = 7). A lower T_p, as compared to PEO, indicates smaller crystallite sizes. T_p varies from 55 to 60°C at these compositions. The width of the endotherm ($T_e - T_o$) gives an idea of the distribution of the crystallite sizes. A lower ΔH_m shows a reduced degree of crystallinity. Because ionic conduction takes place primarily through the amorphous phase of the polymer, low crystallinity is conducive to high conductivity. Literature data [10] indicate that PEO crystallinity is disturbed even at concentrations of $LiBF_4$ as low as O:Li = 50. Also, the endotherms for low lithium concentrations up to O:Li = 7 show broad, skewed patterns indicating a broad distribution of crystallite sizes. The rapid drop of crystallinity, as measured by ΔH_m versus $LiBF_4$ concentration up to O:Li = 7 is shown in Table 1.

TABLE 1

DSC data for polyethylene oxide doped with lithium tetrafluoroborate

Oxygen:Li	Weight fraction of polymer	T_o/°C	T_p/°C	T_c/°C	ΔH_m/ J g^{-1}	Comments
1:0	0	51.1	68.5	77.0	142	Virgin polymer
9:1	0.191	12.3	54.4	65	62.6	Low temp. complex with PEO
8:1	0.210	10.3	58.9	68.3	79.9	Low temp. complex with PEO
7:1	0.233	28.1	60.0	70.5	41.6	Low temp. complex with PEO
6:1	0.262	35.3	57.4	63.0	24.3	Low temp. complex
		80.4	108.6	121	7.2	High temp. complex
5:1	0.299	33.8	58.6	66.2	31.7	Low temp. complex
		97.4	129.5	138.1	21.8	High temp. complex
4:1	0.348	17.9	55.3	70.1	24.4	First heat
		99.0	143.3	156.3	32.5	First heat
		45.4	56.9	62.8	5.4	Second heat
		91.4	139.4	150.3	38.9	Second heat
3:1	0.415	32.2	75.2	118.8	39.0	Low temp. complex
		124.6	151.7	159.9	66.9	High temp. complex
2:1	0.516	70.1	93.6	100.4	32.6	Broad low temp. complex
		118.8	144.4	151.8	45.1	High temp. complex
1:1	0.681 (wt. fraction $LiBF_4$)	40.2	97.8	113.9	157.1	A sharp peak ending in another broad peak
		113.9	136.5	194.4	67.2	
0:1	1.0	84.3	115.8	122.7	282.8	Double peaks
		122.7	131.7	179.4	179.1	Double peaks

Beginning at an O:Li ratio of 6, double endotherms, indicating simultaneous high and low temperature crystalline complexes, are observed. The high temperature complex gets more and more pronounced as the salt concentration increases up to O:Li = 3 (Fig. 2, curve B). Also, ΔH_m for both low and high temperature crystalline complexes progressively increases. At O:LI = 3 (Fig. 2, curve B) a very diffused low temperature endotherm and a highly intense, symmetric high temperature endotherm with a peak at 152°C are observed. The symmetry and sharpness of the latter endotherm indicate highly ordered, narrowly distributed crystallites. Literature data (Table 2) indicate formation of a eutectic at this composition. The morphology of these complexes depends on the thermal history of the samples as will be observed by comparing the first and second runs of the same sample (O:Li = 4) in Fig. 2, curves A and A′. This is

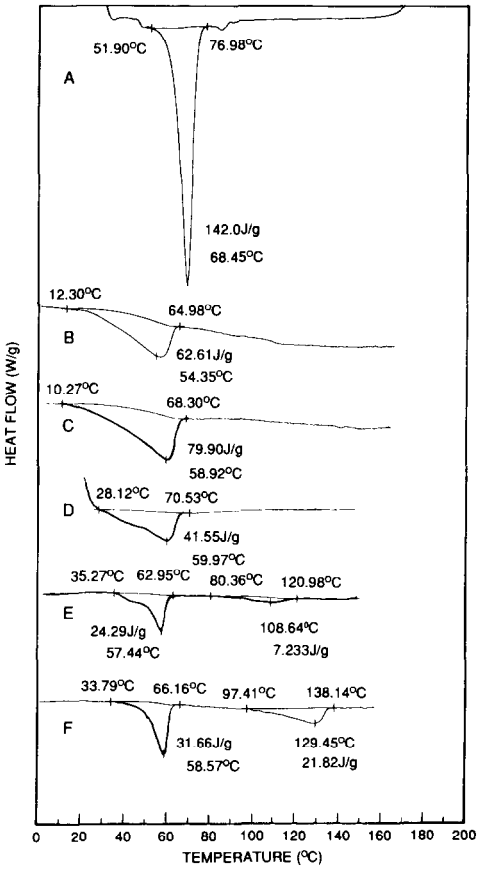

Fig. 1. DSC curves for PEO and PEO–$LiBF_4$ complexes at different dopant concentrations. Curve A, PEO; B, O:Li = 9; C, O:Li = 8; D, O:Li = 7; E, O:Li = 6; F, O:Li = 5.

contrary to the observation of Lee and Wright [11], who observed the same melting temperature for annealed and unannealed samples of PEO–NaSCN, although they observed differences in the lammelar thickness of crystallites by electron microscopy.

At compositions lower than O:Li = 3, unreacted lithium salt exists. The similarity of the shape of the curves for O:Li = 1 (Fig. 2, curve D) and the pure salt (Fig. 2, curve E), although differing in transition temperature, lends support to this conclusion. Double peaks for $LiBF_4$ are due to melting and subsequent decomposition, as confirmed by the TG curve which shows a transition at around 130°C.

In Fig. 3, the peak temperatures for the single and double endotherms are plotted. This represents the approximate phase changes as the weight fraction of lithium increases. Curve A represents the decrease in peak temperature T_p, reflecting lower PEO crystallinity at low lithium concentration. Curve B is a plot of T_p for the lower temperature

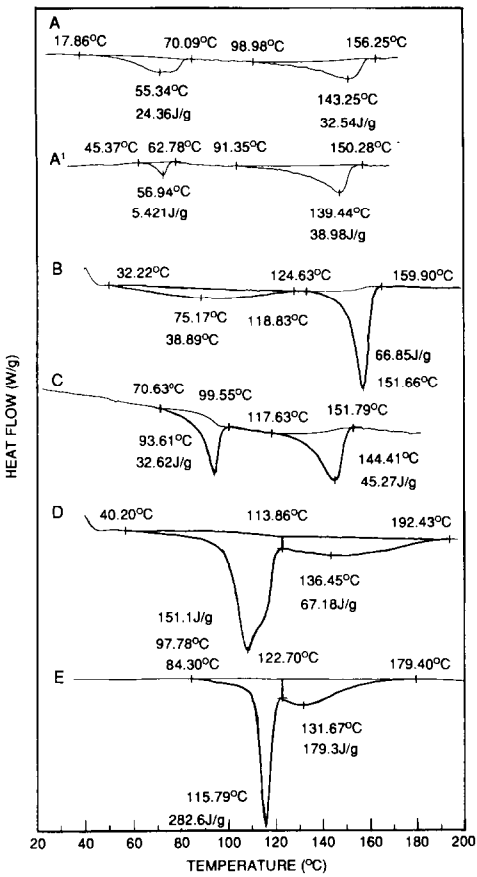

Fig. 2. DSC curves for $LiBF_4$ and PEO–$LiBF_4$ complexes at different dopant concentrations. Curve A, O:Li = 4 (1st scan); A', O:Li = 4 (2nd scan); B, O:Li = 3; C, O:Li = 2; D, O:Li = 1; E, $LiBF_4$.

endotherms of the compositions that have double transitions. This includes the inflexion for O:Li = 7 in Fig. 1. Curves A and B seem to meet together and give a minimum at O:Li = 5, indicating a eutectic composition (Fig. 1, curve F).

Figure 3, curve C, represents the T_p versus composition plot of the higher temperature endotherms for compositions that have double transitions and shows a maximum at O:Li = 3. The sharp, high temperature endotherm at this composition (Fig. 2, curve B) with a peak at 152°C, supports this conclusion. It is interesting that the T_p of the eutectic composition is higher than that of either of the components. A recent study [9] reports the phase diagrams of PEO–$LiBF_4$ and PEO–$LiCF_3SO_3$ using combined X-ray diffraction and DSC. A single phase consisting of a crystalline complex has been reported for PEO–$LiBF_4$ in the range of stoichiometric ratios between 3 and 4 with a eutectic at 3.5. Wright and co-workers [11, 16–18], as well as

TABLE 2

Transition temperatures for different PEO–salt systems

System	Phase II T_1/°C	Phase I T_2/°C	Salt/°C	PEO mol. wt., M_n	Ref.
PEO–NAI ($n = 4$)	–	100	661	–	11
	50–60	–		4×10^6	16
	50–67	195		5×10^6	17
PEO–NaSCN ($n = 4$)	–	170	287	–	11
	50–60	195		4×10^6	16
	50–67	195		5×10^6	17
PEO–KSCN ($n = 4$)	–	170	173	–	11
	100–110	172		4×10^6	16
PEO–$LiCF_3SO_3$ ($n = 4$)	≈60	190	180	5×10^6	19
PEO–$LiCF_3SO_3$ ($n = 3.5$)	–	143	–	5×10^6	9
PEO–$LiBF_4$ ($n = 3.5$)	–	160	–	5×10^6	9
PEO–$LiBF_4$ ($n = 4$)	≈67	160		5×10^6	17
PEO–$LiBF_4$ ($n = 3$)	75	152	111	3×10^5	This work
PEO–$LiBF_4$ ($n = 4$)	54	144	111	3×10^5	This work

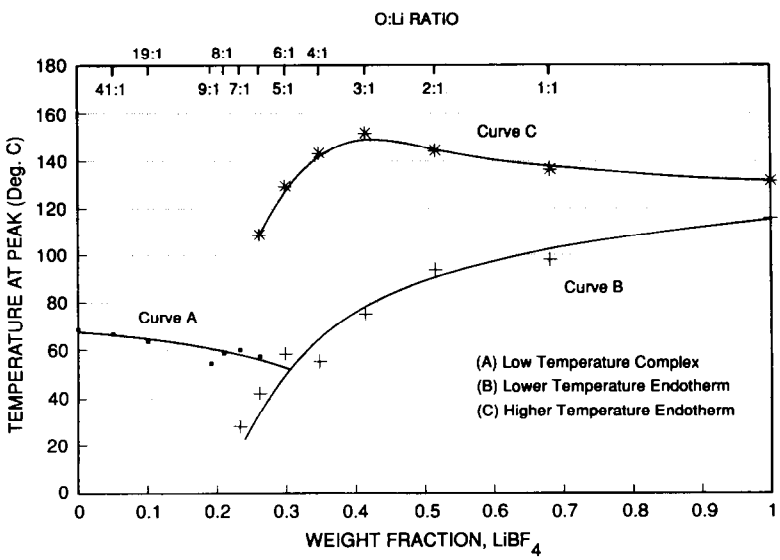

Fig. 3. Peak temperature of PEO–$LiBF_4$ complexes as a function of weight fraction of $LiBF_4$.

Hibma [8], have reported O:Li = 4 as the eutectic composition for a PEO–$LiBF_4$ system with melting points at ≈67°C and 160°C for the lower and higher temperature endotherms, respectively. However, these films were prepared from methanol solution, versus acetonitrile for this work. These authors reported that the morphology of the films can differ by using different preparation methods. Also, the molecular weight of their PEO was much higher (5 000 000) than ours (300 000). These factors may explain the differences in eutectic compositions as well as in the melting points of the crystalline complex. The transition temperatures for the eutectic compositions of Zahurak et al. [9] ($n = 3.5$) and of Wright and co-workers ($n = 4$) are shown in Table 2 along with our data for $n = 3$ and $n = 4$. The latter authors tried to rationalize the two transitions by suggesting the existence of two crystalline phases (I and II). The lower melting temperature of PEO–$LiBF_4$ ($n = 4$) phase I, as compared to the eutectic melting temperatures of other salts, was attributed to the difference in crystalline morphologies and to the lower melting temperature of the pure slat. Nevertheless, it is generally agreed that more than one crystalline intermediate compound is formed, and that the eutectic reaction occurs between PEO and one of the intermediate compounds.

Thermogravimetry

Figure 4, (A) and (B), show the TG/DTG curves for PEO and $LiBF_4$, respectively, in nitrogen. PEO decomposes at a much higher temperature than $LiBF_4$ with a single DTG peak at around 400°C, leaving about 2% residue corresponding to ≈3 parts silica reported by the manufacturer. $LiBF_4$ shows two peaks: the lower temperature peak at around 130°C correlates to the second DSC transition (Fig. 2, curve E) and corresponds to a loss of about one third of the total weight of fluorine. Figure 5 presents TG/DTG curves of a composition with dopant (O:Li = 8). The first peak around 70°C is believed to be due to entrapped solvent. Acetonitrile boils at 81.6°C. The second peak around 280°C is evidently due to the decomposition of $LiBF_4$. The decomposition starts below 150°C, corresponding to the second DSC peak (Fig. 2, curve E). A higher peak temperature as compared to pure $LiBF_4$ (Fig. 4(B)) indicates the higher stability of the complexed salts, validating high T_p values in Fig. 2, curve C. A slight increase in weight at low temperature is evidently due to absorption of moisture during the experiment. As expected, the proportion of residue increases as the $LiBF_4$ ratio increases.

Infrared spectroscopy

Figures 6 (A)–6 (F) show infrared absorption spectra of $LiBF_4$, PEO and PEO–$LiBF_4$ complexes in the 1900–280 cm^{-1} range. Figures 6(A) and 6(B)

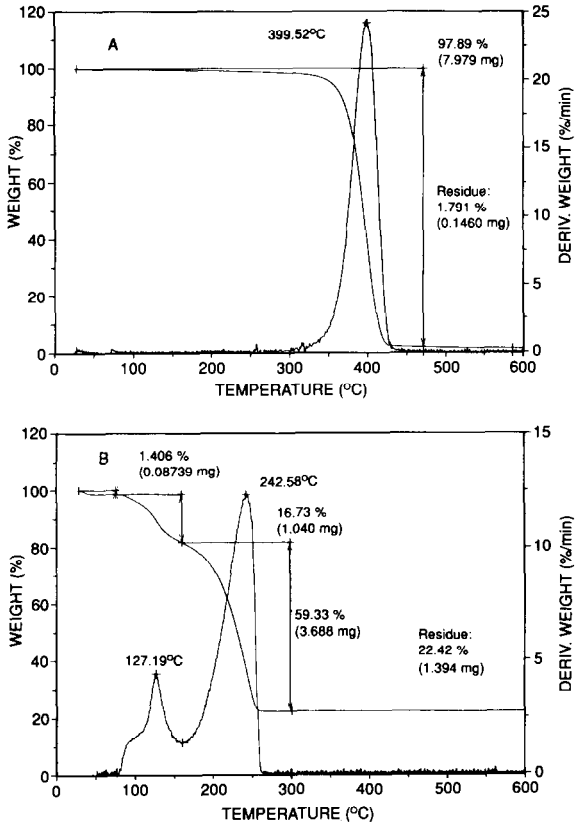

Fig. 4. TG/DTG curves of: (A), PEO; (B), $LiBF_4$.

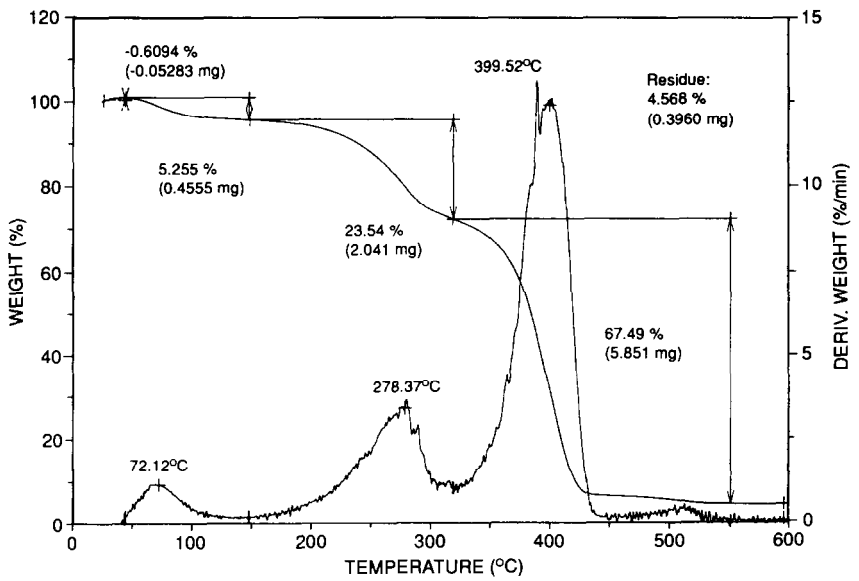

Fig. 5. TG/DTG curve of PEO–$LiBF_4$ complex, O:Li = 8.

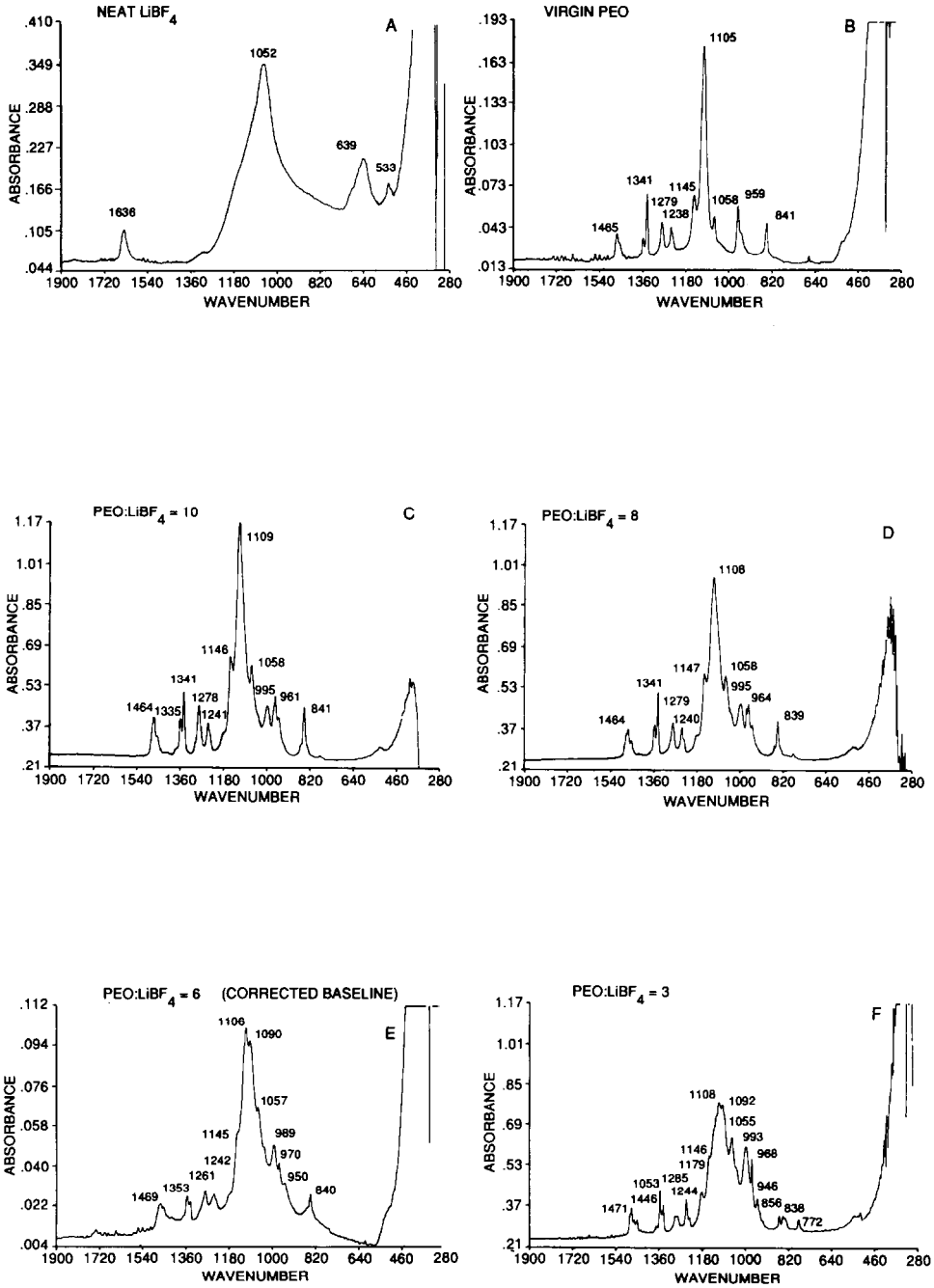

Fig. 6. IR absorption spectra in 1900–280 cm^{-1} region: (A), $LiBF_4$; (B), PEO; (C), O:Li = 10; (D), O:Li = 8; (E), O:Li = 6; (F), O:Li = 3.

correspond to the spectra of $LiBF_4$ and PEO, respectively. The $LiBF_4$ spectrum shows major vibration bands around 1640, 1050, 640 and 530 cm^{-1}, whereas the PEO spectrum shows major bands in the neighborhood of 1465, 1340, 1100, 960, and 840 cm^{-1}. As the proportion of dopant increases, the increased degree of complexation is characterized by band shifts as well as by the formation of new absorption bands. For example, at low dopant concentrations (O:Li = 10 and 8), Figs. 6(C) and 6(D), where DSC shows decreased PEO crystallinity (Table 1), the IR spectral features reveal the predominance of the vibrational bands of PEO and a lack of $LiBF_4$ vibrational features, as expected. However, a new absorption band appears around 995 cm^{-1}, indicating some complexation. Similar IR vibration bands were also observed by Papke et al. [14] for PEO:$LiBF_4$ = 4.5. The 995 cm^{-1} band was ascribed to very strong anion internal mode. Broadening of the 1100 cm^{-1} peak (C–O–C stretching) [14] with dopant concentration, may also indicate lower crystallinity [19] and complexing with oxygen. As the dopant concentration increases further to the range where DSC shows double peaks (O:Li = 6, Fig. 6(E)) some shift of the major PEO peak at 1100 cm^{-1} to lower wavenumber and splitting of the 1100 cm^{-1} peak occur, indicating the development of crystallinity [19]. Finally, at the DSC eutectic composition (O:Li = 3, Fig. 6(F)), some shifts of the existing peaks, development of new peaks, e.g., 860, 996, and 1180 cm^{-1}, and omission of some minor peaks are observed. Splitting of the 1100 cm^{-1} band into sharp bands, Fig. 6(F), indicates further development of crystallinity [19], as expected for a eutectic composition. The 860 cm^{-1} band was tentatively ascribed by Papke et al. [14] to a totally symmetric A_{1g} mode involving a metal–oxygen breathing motion. It was inferred that the PEO chain wraps around the lithium cation.

The absorption spectra in the 3109–2578 cm^{-1} region for PEO, $LiBF_4$ and PEO–$LiBF_4$ complexes are presented in Figs. 7(A)–7(F). $LiBF_4$ (Fig. 7(A)) shows a featureless spectrum, as would be expected for an inorganic compound in this region. PEO (Fig. 7(B)) exhibits a broad C–H stretching band with a peak around 2890 cm^{-1} and inflexions at 2940, 2860, and 2800 cm^{-1}, as well as small absorption bands at 2735 and 2690 cm^{-1}. At low dopant concentrations (O:Li = 8 or 10, Figs. 7(C) and 7(D), the absorption spectra are very similar to the PEO spectrum, with a new absorption peak (inflexion) around 2920 cm^{-1}. The latter is absent in the PEO spectrum and becomes more defined as the dopant concentration increases, with probably a minor shift to lower wavenumbers (Fig. 7(E)). Finally, at the DSC eutectic composition, the new absorption peak seems to split into two well-defined vibration bands at ≈2925 and 2910 cm^{-1}.

The IR spectra presented in Figs. 6(A)–F) and 7(A)–(F) suggest that at low dopant concentrations (O:Li = 8 or 10), the PEO features prevail in the absorption spectra, whereas the features of the crystalline complex (PEO–$LiBF_4$) shows up at higher concentrations. At still higher dopant

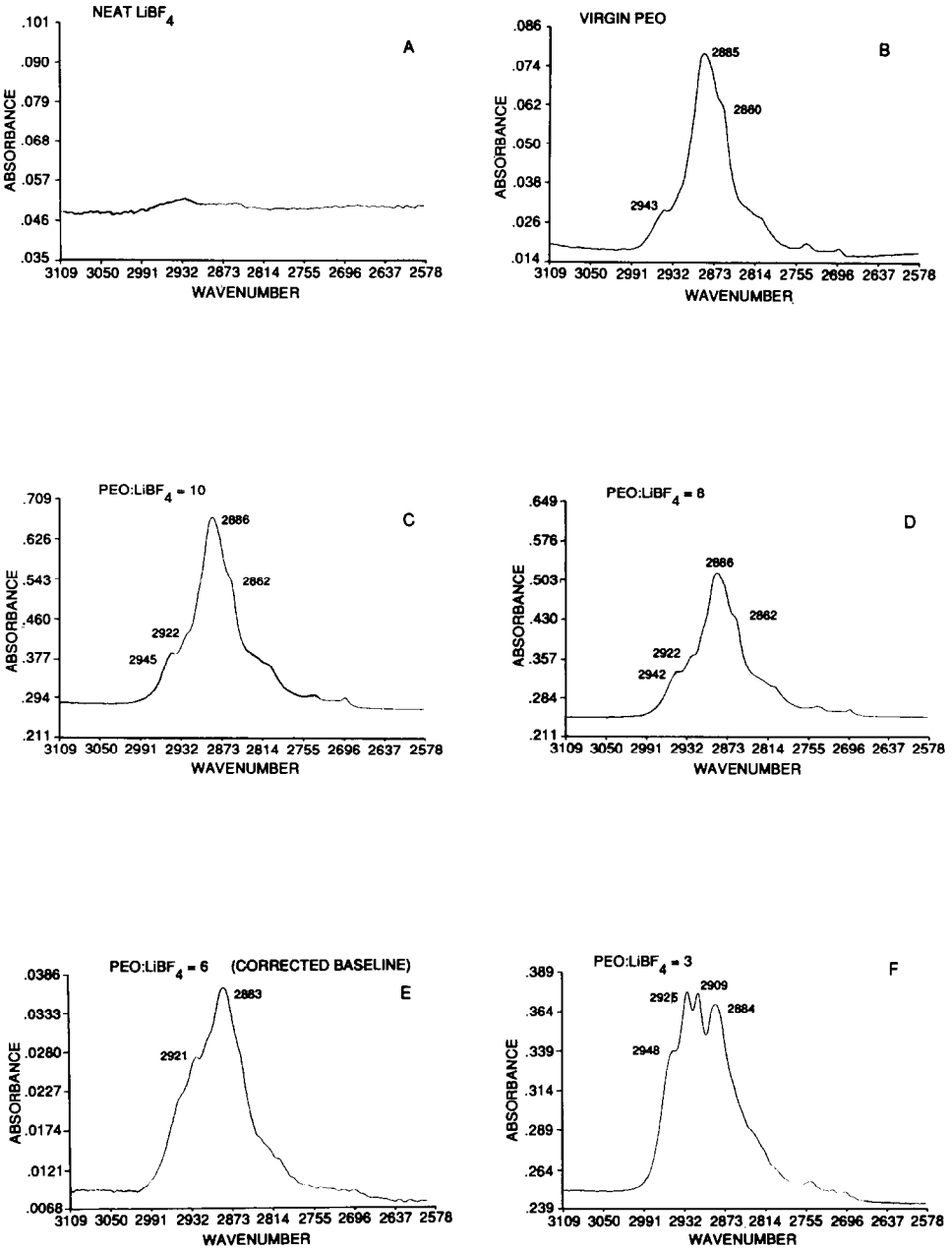

Fig. 7. IR absorption spectra in 3109–2578 cm^{-1} region: (A), $LiBF_4$; (B) PEO; (C) O:Li = 10; (D), O:Li = 8; (E), O:Li = 6; (F), O:Li = 3.

concentration, e.g. O:Li = 2 or 1, not included in the IR study), free $LiBF_4$ (ion pair) remains, as was indicated by DSC. The formation of an ion pair was indicated by Papke et al. [14] in the case of $LiNO_3$ as dopant. Two NO_3 bands arising from nitrate ions in two distinct environments were inferred. Evidence for ion pair interactions has also been presented for the PEO–$NaBH_4$ and PEO–$NaBD_4$ complexes [20].

Conductivity measurements

Figure 8 represents the DEA-generated ionic conductivity data for PEO at different frequencies and temperatures from 20 to 200°C. It may be noted that the curves at 1000 Hz and beyond, converge at temperatures above 80°C. It is believed that at low frequencies electrode polarization gives rise to low conductivity. As the frequency increases, conductivity increases until it approaches a value close to d.c. conductivity. In this work, the conductivity at the maximum available frequency (100 kHz) has been presented as the "apparent conductivity" of the sample.

The conductivity increase at low temperature (up to approx. 70°C) may be correlated to PEO melting. The temperature effect between 70 and 110°C is small. The subsequent small decrease may be due to degradation of $LiBF_4$ as indicated in Fig. 2, curve E, and Fig. 4(B). The apparent room temperature conductivity of virgin PEO at 100 kHz is in the order of $10^{-7.75}$. This value is higher than the literature values of 10^{-9} S cm^{-1} [21, 22], obtained by a "Nyquist plot" of impedance data. Such differences are also

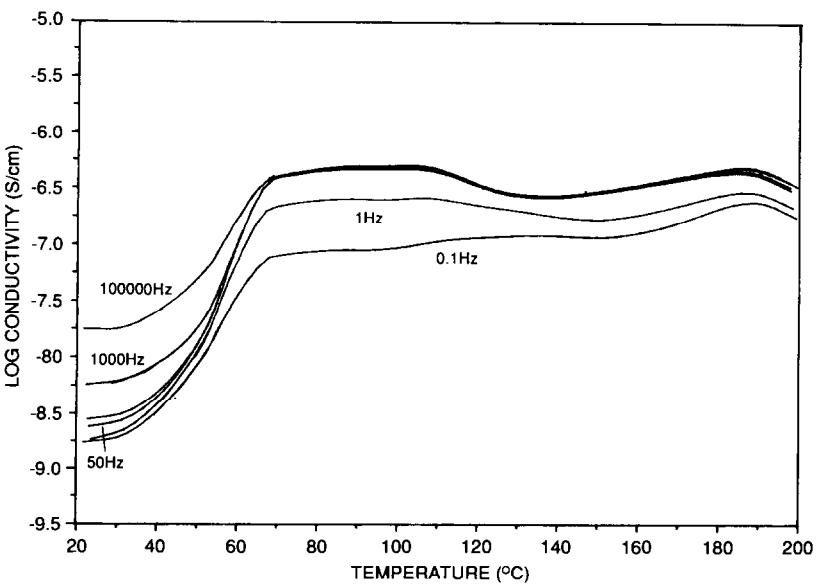

Fig. 8. Ionic conductivities of PEO at different frequencies as a function of temperature.

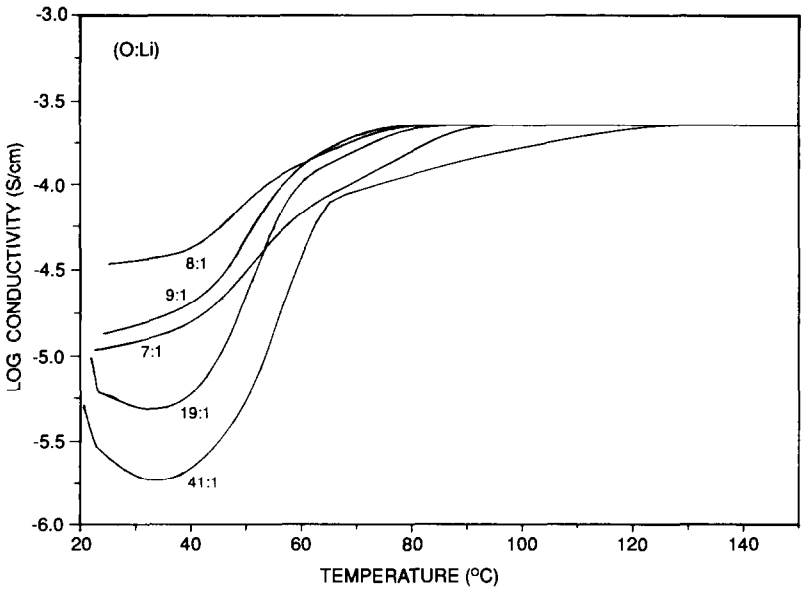

Fig. 9. Apparent ionic conductivity at low dopant concentrations as a function of temperature.

observed for the PEO–LiX complexes reported in Figs. 9 and 10. However, comparative data are still helpful to correlate conductivity with dopant concentration and changes in morphology, as determined by DSC.

In Fig. 9, the apparent conductivity at low dopant concentration is plotted versus temperature. Room temperature conductivity increases as

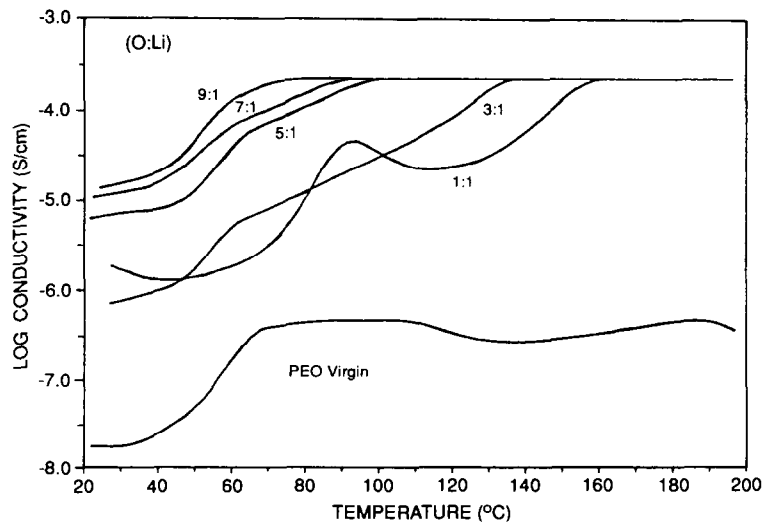

Fig. 10. Apparent ionic conductivity at high dopant concentration as a function of temperature.

dopant concentration increases up to O:Li = 8, and then decreases as the concentration of lithium salt increases further. The latter behavior is further confirmed in Fig. 10 up to a concentration of 1:1 (O:Li).

When a dopant salt is introduced into the polymer matrix, conductivity increases rapidly due to an increased number of charge carriers, despite the viscosity increase, through the growing number of transient crosslinks. However, at large enough concentrations, the viscosity increases and the ion mobility decreases to such an extent that a maximum in conductivity versus salt concentration occurs. It has been suggested [23] that a conductivity drop at higher salt concentration is due not only to the reduced ion mobility but also to the formation of neutral ion pairs (free salt) which decrease the number of charge carriers attached to the polymer and therefore reduce conductivity. In polyethers, as in PEO, the low dielectric constant ($\varepsilon = 5$) favors an extensive ion–ion interaction. Therefore, to optimize conductivity, a compromise between the number of charge carriers, i.e. salt concentration, and their mobility must be made. Figures 9 and 10 indicate that this compromise seems to be achieved at O:Li = 8. This is in agreement with MacCallum and Vincent [24] who report that conductivity increases as O:Li ratio decreases from 50 to 8 and decreases as the salt concentration is raised still further. Recent work by Zahurak, et al. [9] confirms this observation.

Conductivity values also parallel DSC data for crystallinity (ΔH_m) in Table 1, except that the maximum conductivity is at O:Li = 8 instead of 7, as expected from the decrease in ΔH_m data. However, a slight inflection of the DSC endotherm for O:Li = 7 (Fig. 1, curve D) indicates the beginning of a separate phase, which may have affected conductivity. With further increase in dopant concentration up to O:Li = 3 (Figs. 1 and 2), the formation of a separate phase with high temperature crystallinity causes conductivity to decrease. Finally, ion pair formation occurs at higher concentration, affecting conductivity as shown in Fig. 11 (O:Li = 1).

The conductivity rise in Fig. 10 shows a sigmoidal curve with an inflection at around 35–50°C. The inflection may represent melting of the low temperature crystallites. The polymer complex with O:Li = 1 shows a curve that is different from the others, probably due to excess $LiBF_4$ in the system. All the curves converge to a maximum conductivity point, and then show no change in conductivity with temperature. This suggests that the maximum conductivity reached is the limit for the DEA 2970 instrument. Consultation with the manufacturer's representative confirms this view.

Figure 11 shows the effect of lithium concentration at different temperatures on conductivity. Conductivity increases with temperature. Both crystalline PEO and the dopant-rich crystalline complex in the bulk sample suppress conductivity. A high temperature should not only decrease crystallinity but should also increase both the dissociation of ions and their mobility, thus explaining the higher conductivity.

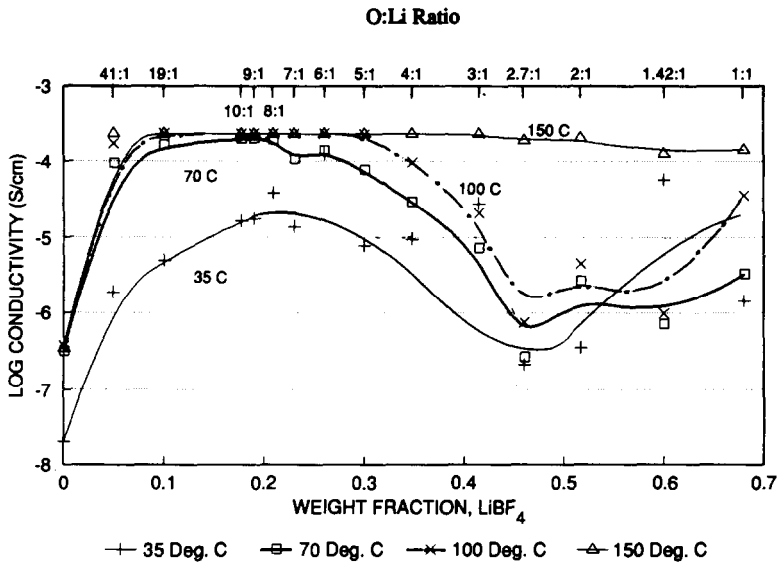

Fig. 11. Apparent logic conductivity at different temperatures as a function of weight fraction of $LiBF_4$.

Dielectric constants measurements

Figure 12 shows the permittivity plots corresponding to the conductivity data in Fig. 9. Permittivity variations with the solid and molten PEO (Fig. 12) show changes similar to those of Porter and Boyd [25]. Literature

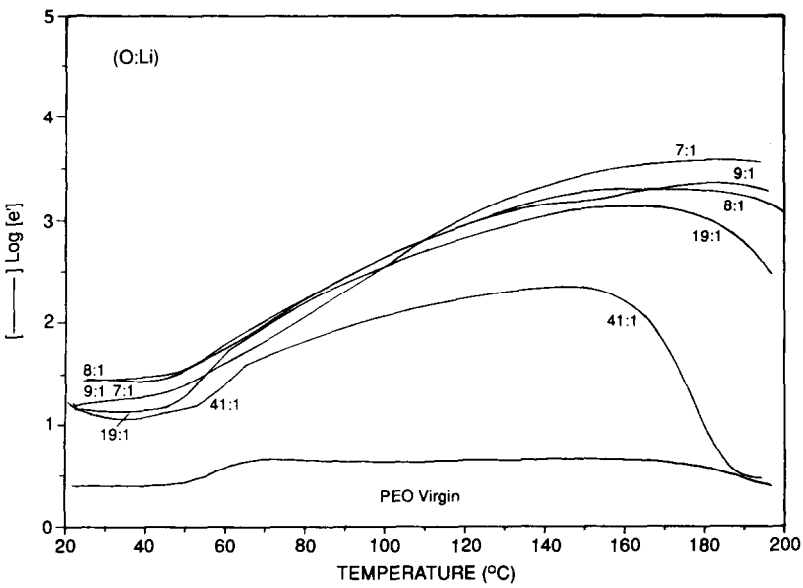

Fig. 12. Permittivity of low $LiBF_4$ concentration as a function of temperature.

values [26] of the room temperature dielectric constant ($\varepsilon = 5$) and molten PEO ($\varepsilon = 8$) agree with the data presented in Fig. 12.

Permittivity data at high frequency at different $LiBF_4$ concentrations (not shown) generally corroborate the conductivity data at high frequencies. As for conductivity, permittivity increases with higher dopant concentration, then decreases as the concentration is increased beyond O:Li = 8. Increasing temperature causes permittivity to increase to a maximum, then to decrease thereafter. The decrease takes place at a higher temperature as the concentration of dopant increases and may be ascribed to the decomposition of the PEO–lithium salt complex. Much of the explanations suggested for conductivity also hold true for permittivity. However, in the case of the permittivity, the data are still within the measurement limits of the instrument except for very high temperatures and concentrations (above 150°C for O:Li = 3 and 170°C for O:Li = 1). These temperatures are at the melting temperature of the eutectic at 3:1 (Fig. 3, curve C) and over the decomposition temperature of the PEO–lithium salt complex (1:1 Fig. 2, curve D) and the data collected at these temperatures have little practical significance.

CONCLUSIONS

The highest ionic conductivity in PEO–$LiBF_4$ complexes is achieved at O:Li = 8. The ionic conductivity of PEO–$LiBF_4$ complexes at dopant concentrations of less than O:Li = 8 is reduced because of the formation of more than one crystalline complex.

DEA offers some advantages for evaluating the polymeric electrolytes of solid polymer batteries. The main advantage is the speed at which a large amount of computerized data may be generated, as a function of both temperature and frequency and the enclosed environment it provides. The limitation of DEA is its limited measurement range. This limit is in the range of 10–3.5 S cm^{-1}. Also, the apparent conductivity is higher than that obtained previously by impedance measurements. The measurement ceiling does not apply for permittivity measurements.

DSC and TG/DTG data show the temperatures for phase transitions and stability of the components and compounds, and help to explain the data generated by DEA. FTIR spectra give further insight into the PEO–$LiBF_4$ complex morphologies and generally support the observations obtained from DSC data.

ACKNOWLEDGMENTS

The authors thank Mr. Jonathan A. Foreman of TA Instruments, Inc. for consultations during the course of this investigation. Thanks are also due to Dr. L. Scanlon of WPAFB for helpful criticism, Dr. S.M. Linden for consultation on IR spectra, Ms. Ruth Rodak for editorial comments, and to

Mrs. Jeanne Miller for secretarial help. The work was financed by the Aeropropulsion and Power Directorate of the Wright-Patterson Air Force Base (WPAFB) under Contract No. F33615-90-C-2036. The authors are grateful to WPAFB for permission to publish this paper.

REFERENCES

1 M.B. Armand, J.M. Chabago and M. Duelot, in P. Vashishta, J.N. Mundy and G.K. Shenoy (Eds.), Fast Ion Transport in Solids, North Holland, New York, 1979.
2 D. Fauteux, in J.R. MacCallum and C.A. Vincent (Eds.), Polymer Electrolyte Reviews-1, Elsevier Applied Science, London and New York, 1987, p. 121.
3 M. Minier, C. Berthier and W. Gorecki, Solid State Ionics, 9/10 (1983) 1125.
4 P.R. Sorensen and T. Jacobsen, Polym. Bull., 9 (1983) 47.
5 D. Fauteux, M.D. Lupien and C.D. Robitailee, J. Electrochem. Soc., 134 (1987) 2761.
6 P. Ferloni, G. Chiodelli, A. Magistris and M. Sanesi, Solid State Ionics, 18/19 (1986) 265.
7 C.D. Robitaille and D. Fauteux, J. Electrochem. Soc., 133 (1986) 315.
8 T. Hibma, Solid State Ionics, 9/10 (1983) 1101.
9 S.M. Zahurak, M.L. Kaplan, E.A. Rietmann, D.W. Murphy and R.J. Cava, Macromolecules, 21 (1988) 654.
10 Y.L. Lee and B. Crist, J. Appl. Phys., 60 (1986) 2683.
11 C.C. Lee and P.V. Wright, Polymer, 23 (1982) 681.
12 M. Minier, C. Berthier and W. Gorecki, J. Phys. (Paris), 45 (1984) 739.
13 C. Berthier, W. Gorecki, M. Minier, M.B. Armand, J.M. Chabagno and P. Rigaud, Solid State Ionics, 11 (1983) 91.
14 B.L. Papke, M.A. Ratner and D.F. Shriver, J. Electrochem. Soc., 129 (1982) 1434.
15 Literature on DEA 2970, TA Instruments, New Castle, DE 19720.
16 D.E. Fenton, J.M. Parker and P.V. Wright, Polymer, 14 (1973) 589.
17 P.V. Wright, Br. Polym. J., 7 (1975) 319.
18 D.R. Payne and P.V. Wright, Polymer, 23 (1982) 690.
19 J. Haslam and H.A. Willis, Identification and Analysis of Plastics, D. Van Nostrand Co., Inc., London, 1965, p. 246.
20 B.L. Papek, R. Dupon, M.A. Ratner and D.F. Shriver, Solid State Ionics, 5 (1981) 685.
21 J.S. Tonge and D.F. Shriver, in J.H. Lai (Ed.), Polymers for Electronic Applications, CRC Press, 1989, pp. 185–187.
22 F.M. Gray, in Solid Polymer Electrolytes, Fundamentals and Technological Applications, VCH Publishers, Inc., New York, 1991, 39.
23 L.M. Torell and S. Schantz, in J.R. MacCallum and C.A. Vincent (Eds.), Polymer Electrolyte Review-2, Elsevier Applied Science, London and New York, 1989, Chapt. 1.
24 J.R. MacCallum and C.A. Vincent, Polymer Electrolyte Reviews-1, Elsevier Applied Science, London and New York, 1987, pp. 24, 32.
25 C.H. Porter and R.H. Boyd, Macromolecules, 4 (1971) 589.
26 M.C. Wintersgill and J.J. Fontanella, in J.R. MacCallum and C.A. Vincent (Eds.) Polymer Electrolyte Reviews-2, Elsevier Applied Sciences, London, 1989, p. 46.